

# Baryonic models of ultra-low-mass compact stars for the central compact object in HESS J1731-347

Jia Jie Li<sup>a</sup>, Armen Sedrakian<sup>b,c</sup>

<sup>a</sup>*School of Physical Science and Technology, Southwest University, Chongqing 400715, China*

<sup>b</sup>*Frankfurt Institute for Advanced Studies, D-60438 Frankfurt am Main, Germany*

<sup>c</sup>*Institute of Theoretical Physics, University of Wrocław, 50-204 Wrocław, Poland*

## Abstract

The recent attempt on mass and radius inference of the central compact object within the supernova remnant HESS J1731-347 suggests for this object an unusually low mass of  $M = 0.77^{+0.20}_{-0.17} M_{\odot}$  and a small radius of  $R = 10.4^{+0.86}_{-0.78}$  km. We explore the ways such a result can be accommodated within models of dense matter with heavy baryonic degrees of freedom which are constrained by the multi-messenger observations. We find that to do so using only purely nucleonic models, one needs to assume a rather small value of the slope of symmetry energy  $L_{\text{sym}}$ . Once heavy baryons are included higher values of the slope  $L_{\text{sym}}$  become acceptable at the cost of a slightly reduced maximum mass of static configuration. These two scenarios are distinguished by the particle composition and will undergo different cooling scenarios. In addition, we show that the universalities of the  $I$ -Love- $Q$  relations for static configurations can be extended to very low masses without loss in their accuracy.

**Keywords:** Equation of state, Heavy baryons, Compact stars, Supernova remnant

## 1. Introduction

Over the last decade, there has been exciting progress in gathering new astrophysical information on compact star (CS) parameters such as mass, radius, and tidal deformability. This progress boosts the search for the ultimate state of dense matter and, simultaneously, narrows down the admissible theories of dense matter.

The most massive neutron star yet observed, PSR J0740+6620, with a mass of  $2.08^{+0.07}_{-0.07} M_{\odot}$  (68.3% CI) [1, 2], excludes equation of state (EoS) models which cannot support star with masses that reach that limit. Recently the companion of “black widow” pulsar PSR J0952-0607 was reported to have a mass of  $2.35^{+0.17}_{-0.17} M_{\odot}$  (68.3% CI) [3], which makes it the fastest and heaviest known neutron star to date. The data from the NICER instrument and pulse modelling of X-ray emission from hot spots on the surfaces of CSs have provided simultaneous mass and radius measurements for PSR J0030+0451 [4, 5] and PSR J0740+6620 [6, 7]. The detection of gravitational wave (GW) event GW170817 [8] involving a merger of two CSs has placed constraints on the tidal deformability of this system,  $\tilde{\Lambda} \leq 720$  [9–13]. While the associated electromagnetic counterparts, AT2017gfo and GRB170817A [14, 15], have provided an upper limit on the maximum static mass of neutron stars  $M \sim 2.3 M_{\odot}$  [16–21]. The X-ray observations of the temperature of the neutron star in the Cassiopeia A supernova remnant and modeling of its thermal evolution give insights into the superfluid properties of the core matter (see Ref. [22] and references therein).

Very recently, an estimate of the mass and radius of the central compact object (CCO) within the supernova remnant HESS J1731-347 was reported [23] using modeling of its X-ray spectrum and a distance estimate from Gaia observations. The mass and the radius of this object are  $M = 0.77^{+0.20}_{-0.17} M_{\odot}$  and  $R = 10.4^{+0.86}_{-0.78}$  km (68.3% CI), respectively, when only parallax priors and X-ray data are considered. Taking in addition the full distance priors and EoS constraint priors into account, the improved estimates are  $M = 0.83^{+0.17}_{-0.13} M_{\odot}$  and  $R = 11.25^{+0.53}_{-0.37}$  km (68.3% CI). This estimation makes the CCO in HESS J1731-347 the lightest neutron star known to date [23, 24], and potentially a candidate for an exotic object — “strange star” [23, 25, 26], as stars made of ordinary matter in supernova explosions have a lower limit on the mass which is above  $1.17 M_{\odot}$  [27]. Previously, the confirmed lightest neutron star with  $M = 1.174^{+0.004}_{-0.004} M_{\odot}$  is the companion star in the double neutron star system with the primary being the pulsar J0453+1559 which has an estimated mass [28, 29]. Note that these two mass estimates are compatible at better than  $2\sigma$  accuracy.

Ref. [23] based their discussion on EoS models and associated mass-radius ( $M$ - $R$ ) curves which were based on the  $\chi$ EFT EoS up to the density of  $1.5\rho_{\text{sat}}$  (where  $\rho_{\text{sat}}$  is the nuclear saturation density) that are extrapolated to higher densities using the constant speed-of-sound EoS. It was shown that a large number of EoS models meets all current observational constraints. An alternative scheme of analysis is based on the covariant density functional (CDF) approach [30, 31], which is a powerful tool that allows one to model finite nuclei and nuclear matter across a wide range of densities and temperatures relevant to neutron stars and their coalescences. In this work, we test how well the CDF approach to baryonic matter can accommodate the pu-

Email addresses: jiajieli@swu.edu.cn (Jia Jie Li), sedrakian@fias.uni-frankfurt.de (Armen Sedrakian)

tative mass and radius values inferred for the CCO in HESS J1731-347 by Ref. [23].

## 2. CDF for baryonic matter

The theoretical framework implemented in this work has been presented in great detail in Ref. [31]. We provide below the most relevant points of our approach for the sake of completeness. The baryonic matter is described within a CDF approach with density-dependent baryon-meson couplings [31, 32]. The interaction part of the Lagrangian is given by

$$\begin{aligned} \mathcal{L}_{\text{int}} = & \sum_B \bar{\psi}_B \left( -g_{\sigma B} \sigma - g_{\sigma^* B} \sigma^* - g_{\omega B} \gamma^\mu \omega_\mu - g_{\phi B} \gamma^\mu \phi_\mu \right. \\ & \left. - g_{\rho B} \gamma^\mu \vec{\rho}_\mu \cdot \vec{\tau}_B \right) \psi_B + \sum_D (\psi_B \rightarrow \psi_D^*), \end{aligned} \quad (1)$$

where  $\psi$  stands for the Dirac spinor with index  $B$  labeling the spin-1/2 baryonic octet, namely, nucleons  $N \in \{n, p\}$  and hyperons  $Y \in \{\Lambda, \Xi^{0,-}, \Sigma^{+,0,-}\}$ , while  $\psi^\nu$  for the Rarita-Schwinger spinor [33] with index  $D$  referring to the spin-3/2 resonance quartet  $\Delta \in \{\Delta^{++}, \Delta^+, \Delta^0, \Delta^-\}$ . The baryons interact via exchanges of  $\sigma, \omega$  and  $\rho$  mesons, which comprise the minimal set necessary for a quantitative description of nuclear phenomena [34]. In addition, the two hidden-strangeness mesons ( $\sigma^*, \phi$ ) describe interactions between hyperons [35–37].

In the nucleonic sector, these are three meson-nucleon ( $mN$ ) coupling constants ( $g_{\sigma N}, g_{\omega N}, g_{\rho N}$ ) at saturation density  $\rho_{\text{sat}}$ , and four parameters that control their density dependence. These seven parameters allow one to establish the correspondence between this type of a CDF and the purely phenomenological expansion of the energy density of nuclear matter [38, 39] in the vicinity of  $\rho_{\text{sat}}$ , with respect to the number density  $\rho$  and isospin asymmetry  $\delta = (\rho_n - \rho_p)/\rho$  where  $\rho_{n(p)}$  is the neutron (proton) density. The coefficients of this double expansion are referred to commonly as saturation energy  $E_{\text{sat}}$ , incompressibility  $K_{\text{sat}}$ , and the skewness  $Q_{\text{sat}}$  in isoscalar channel, and the symmetry energy  $J_{\text{sym}}$ , and its slope parameter  $L_{\text{sym}}$  in isovector channel.

Among the above-mentioned coefficients, of particular interest are the quantities that arise at a higher order of the expansion, specifically,  $Q_{\text{sat}}$  and  $L_{\text{sym}}$ . Their values are weakly constrained by the conventional fitting protocol used in constructing the density functionals. However, they play complementary roles as the value of  $Q_{\text{sat}}$  controls the high-density behavior of the nucleonic EoS, and thus the maximum mass of nucleonic CSs, while the value of  $L_{\text{sym}}$  determines the intermediate-density behavior of the nucleonic EoS, and thus the radii of low-mass stars.

In hyperonic sector, the vector meson-hyperon ( $mY$ ) couplings are given by either the SU(6) spin-flavor symmetric quark model or the SU(3) flavor symmetric model [31, 35–37], depending on the stiffness of the utilized nucleonic EoS model. On the other hand the scalar meson-hyperon couplings are determined by fitting to certain preselected properties of hypernuclear systems. To be specific, as it is common, we determine the coupling constants,  $g_{\sigma Y}$ , using the following hyperon potentials

in the symmetric nuclear matter at  $\rho_{\text{sat}}$  [40, 41]:

$$U_\Lambda^{(N)} = -U_\Sigma^{(N)} = -30 \text{ MeV}, \quad U_\Xi^{(N)} = -14 \text{ MeV}. \quad (2)$$

In addition, we adopt the  $\Lambda\Lambda$  bond energy at  $\rho_{\text{sat}}/5$ , which reproduces the most accurate experimental value to date [42],

$$U_\Lambda^{(\Lambda)} = -0.67 \text{ MeV}, \quad (3)$$

to fix the value of the coupling  $g_{\sigma^* \Lambda}$ . The coupling of remaining hyperons  $\Xi$  and  $\Sigma$  to the  $\sigma^*$  is determined by the relation  $g_{\sigma^* Y}/g_{\phi Y} = g_{\sigma^* \Lambda}/g_{\phi \Lambda}$  [37].

Finally, let us turn to the  $\Delta$ -resonance sector. The information on the meson- $\Delta$  ( $m\Delta$ ) couplings is scarce, as no consensus has been reached yet on the magnitude of the  $\Delta$  potential. In this work, we limit ourselves to the case where

$$R_{\Delta\omega} = g_{\omega\Delta}/g_{\omega N} = 1.1, \quad R_{\Delta\rho} = g_{\rho\Delta}/g_{\rho N} = 1.0, \quad (4)$$

and  $R_{\Delta\sigma} = g_{\sigma\Delta}/g_{\sigma N}$  is determined by fitting to the following representative values of  $\Delta$ -potentials in nuclear matter at  $\rho_{\text{sat}}$ ,

$$U_\Delta^{(N)} = 1, 4/3, 5/3 U_N, \quad (5)$$

where  $U_N$  is the nucleon isoscalar potential. This means the potential of  $\Delta$ 's in the nuclear medium is more attractive than the nucleon potential, consistent with the studies of the scattering of electrons and pions off nuclei and photoabsorption with phenomenological models [43]. The resultant values for  $R_{\Delta\sigma}$ , respectively, are,

$$R_{\Delta\sigma} \simeq 1.10, 1.16, 1.23. \quad (6)$$

Note that within the range ( $R_{\Delta\sigma} - R_{\Delta\omega}$ )  $\geq 0.15$ ,  $\Delta$ -admixed matter undergoes spinodal instability [44]. Our choice avoids such instabilities with the most attractive case  $U_\Delta^{(N)} = 5/3 U_N$  being at the limit of the stability. This completes our discussion of the parameters entering our CDF for baryonic matter and they are now fully determined. Note that we assume that the hyperon and  $\Delta$  potentials scale with a density as the nucleonic one, therefore their high-density behavior is inferred from that of the nucleons.

With this input, we compute the EoS of the stellar matter by implementing the additional conditions of weak equilibrium and charge neutrality that prevail in CSs. We further match smoothly our EoS for the core to that of the crust EoS given in Refs. [45, 46] at the crust-core transition density  $\sim \rho_{\text{sat}}/2$ .

In the present work, as in Refs. [39, 47], we map the nucleonic EoS given by the Lagrangian (1) for each set of parameters  $Q_{\text{sat}}$  and  $L_{\text{sym}}$ . For our analysis below we adopt the lower-order coefficients in the isoscalar channel, i.e.,  $E_{\text{sat}} = -16.14$ , and  $K_{\text{sat}} = 251.15 \text{ MeV}$ , as those inferred from the DDME2 parametrization [32] which were adjusted to the properties of finite nuclei. For the isovector channel, instead fixing  $J_{\text{sym}} = 32.31 \text{ MeV}$  the DDME2 value, we hold the value of the symmetry energy at a lower density  $\rho_c = 0.11 \text{ fm}^{-3}$  at the constant value  $E_{\text{sym}}(\rho_c) = 27.09 \text{ MeV}$  [39]. The density  $\rho_c$  is distinguished by the fact that a large variety of nuclear models predict almost identical values of  $E_{\text{sym}}(\rho_c)$ . In the following discussion, we will use the pair of parameters ( $Q_{\text{sat}}, L_{\text{sym}}$ ) to identify any specific nucleonic CDF.

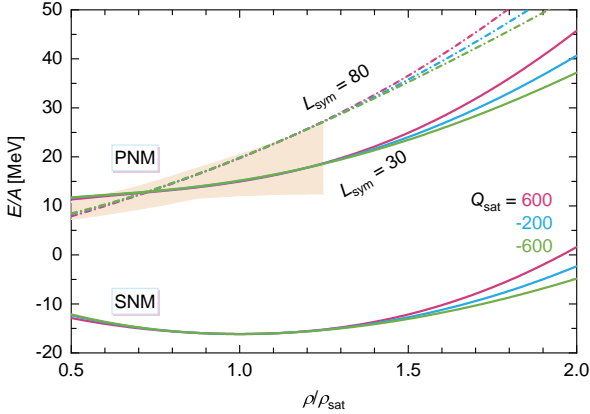


Figure 1: Energy per particle of symmetric nucleonic matter (SNM) and pure neutron matter (PNM) as a function of density  $\rho/\rho_{\text{sat}}$ , obtained from six representative  $(Q_{\text{sat}}, L_{\text{sym}})$  pairs (in MeV). The band corresponds to the combined  $\chi$ EFT results from Ref. [48].

To appreciate the quality of current functional and the range of variation of parameters we show in Fig. 1 the energy per particle of symmetric nucleonic matter (SNM) and pure neutron matter (PNM) as a function of density for six representative  $(Q_{\text{sat}}, L_{\text{sym}})$  pairs, while keeping all other coefficients at their default values of DDME2 parametrization [32, 39]. We further restrict the set of EoS by choosing only those which reproduce the combined result for PNM derived from several recent many-body calculations with  $\chi$ EFT interactions for densities up to  $\sim 1.3\rho_{\text{sat}}$  [48]. This results in the range  $30 \leq L_{\text{sym}} \leq 80$  MeV, which is independent of the values of  $Q_{\text{sat}}$ . In addition, we have checked that all the alternative parametrizations can reasonably reproduce the binding energies and charge radii of several closed-shell nuclei with  $\sim 2\%$  relative deviation.

### 3. Results and discussion

#### 3.1. CSs with only nucleons

We start our discussion with the CS models containing only nucleons. We limit the discussion to three sets of representative EoS models by taking three values of  $Q_{\text{sat}} = -600, -200,$  and  $600$  MeV, and a range of  $L_{\text{sym}}$  which allow an overlap of our models with the range limited by the analysis of the CCO in HESS J1731-347 [23]. Large values of  $L_{\text{sym}}$  correspond to a stiffer EoS close to nuclear saturation density, as shown in Fig. 1, and lead to larger radii for low-mass stars. Larger values of  $Q_{\text{sat}}$  imply EoS which are stiffer at high density and, thus, predict larger maximum masses for static nucleonic stars [39, 49]. For  $Q_{\text{sat}} = -600$  MeV the maximum mass is about  $2.0 M_{\odot}$ , which matches the mass of PSR J0740+6620 [1, 2]; for  $Q_{\text{sat}} = -200$  MeV the maximum mass is consistent with the (approximate) *theoretical upper limit* on the maximum mass of static CSs  $\sim 2.3 M_{\odot}$  inferred from analysis of the GW170817 event and the corresponding electromagnetic counterparts in a scenario where a supramassive remnant formed after a merger collapses into a black hole [16–21]; finally, for  $Q_{\text{sat}} = 600$  MeV the maximum mass is slightly higher than  $2.5 M_{\odot}$ , which would be

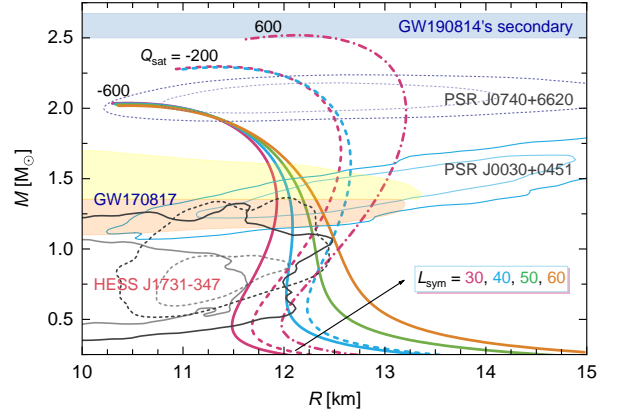


Figure 2:  $M$ - $R$  relation for nucleonic EoS models with different pairs of values of  $Q_{\text{sat}}$  and  $L_{\text{sym}}$ . We show three branches of  $M$ - $R$  curves, for  $Q_{\text{sat}} = -600$  (solid lines),  $-200$  (dashed lines) and  $600$  MeV (dash-dotted lines). For each of these,  $L_{\text{sym}}$  is varied from  $30$  MeV to larger values that are still compatible with the ellipse of HESS J1731-347 at 95.4% CI. The shaded regions show the constraints from analysis of GW events [9, 50], the ellipses indicate the regions compatible with the inferences from NICER observations [4–7], the contours show the  $M$ - $R$  constraints for the CCO in HESS J1731-347 [23]. See text for details.

compatible with the mass of the secondary in the GW190814 event [50] and its interpretation as a nucleonic CS [51–53].

The  $M$ - $R$  relations for our nucleonic EoS models are shown in Fig. 2, along with the current astrophysical observational bands derived from X-ray or gravitational wave observations. These include: (i) the ellipses obtained by the NICER collaboration which simultaneously determined the radius and mass of PSR J0030+0451 and J0740+6620 via X-ray pulse-profile modeling (at 68.3% and 95.4% CIs) [4–7]; (ii) the  $M$ - $R$  contours for the CCO in HESS J1731-347, where solid lines correspond to the case that only parallax priors and X-ray data are considered, and the dashed lines correspond to the joint fit including all prior information (at 68.3% and 95.4% CIs) [23]; (iii) the regions for each of the two CSs that merged in the GW170817 event (at 90% CIs) [10]; and (iv) the mass of the secondary component of the GW190814 event (at 90% CI) [50].

As seen from Fig. 2, these observational ellipses can be accounted for by appropriate choices of the parameters  $Q_{\text{sat}}$  and  $L_{\text{sym}}$  at the 95.4% CI. The choice of these parameters gives sufficient flexibility to allow for intermediate-density soft EoS to account for ellipses for CCO in HESS J1731-347 and GW170817 and sufficiently stiff EoS at high density to account for the ellipses of PSR J0740+6620. To give more specific examples, a 95.4% CI consistency is achieved by choosing  $L_{\text{sym}} \leq 60$  MeV and  $Q_{\text{sat}} \sim -600$  MeV,  $L_{\text{sym}} \leq 40$  MeV and  $Q_{\text{sat}} \sim -200$  MeV, and  $L_{\text{sym}} \leq 30$  MeV and  $Q_{\text{sat}} \sim 600$  MeV. Among these, the model with  $(Q_{\text{sat}}, L_{\text{sym}}) = (-600, 30)$  MeV intersects also the 68.3% CI ellipse. Thus, we conclude that the nucleonic models are consistent with the current information available from multimessenger astrophysics within 95.4% CI, in particular, the small radius of the CCO in HESS J1731-347, *if fairly low values of  $L_{\text{sym}}$  are adopted*. These low values for  $L_{\text{sym}}$  lie outside the  $1\sigma$  confidence placed by the analysis of neutron skin in the PREX-II experiment for  $^{208}\text{Pb}$  [54, 55], but are compatible

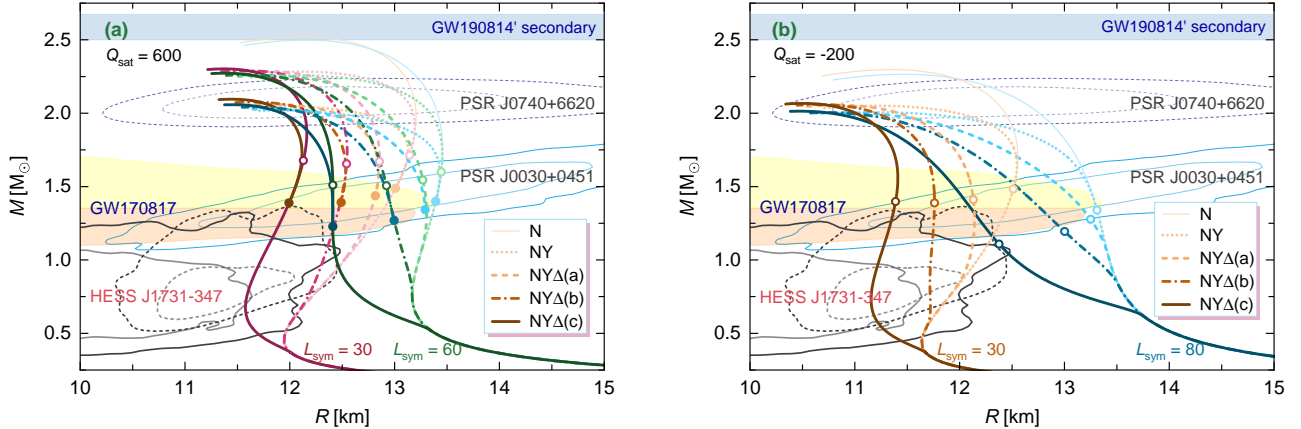


Figure 3:  $M$ - $R$  relation for hyperon- $\Delta$  admixed EoS models for different  $\Delta$  potential depths at nuclear saturation density  $U_{\Delta}/U_N = 1, 4/3, 5/3$ , which are labeled as “NY $\Delta$ (a)-(c)”, respectively. The results for purely nucleonic and hyperonic EoS models are also shown. In panel (a) the EoS models are constructed from the nucleonic model with pairs of  $(Q_{\text{sat}}, L_{\text{sym}}) = (600, 30)$  and  $(600, 60)$  MeV, combined with either SU(6) or a SU(3) symmetric model for the hyperonic sector. In panel (b) the EoS models are constructed from the nucleonic model with pairs of  $(Q_{\text{sat}}, L_{\text{sym}}) = (-200, 30)$  and  $(-200, 80)$  MeV and a SU(3) symmetric parametrization of the hyperonic sector. The onset mass of hyperons for each EoS model is marked by circles. See text for details.

with the analysis including also dipole polarizabilities in a set of finite nuclei [56], the analysis of the CREX experiment for  $^{48}\text{Ca}$  [57, 58], as well as with recent  $\chi$ EFT predictions [59].

A large sample of nucleonic EoS based on CDF theory with nonlinear couplings was considered in Ref. [24] and was found to be inconsistent with the 68.3% CI ellipses of HESS J1731-347. This is in contrast to our finding, even though our EoS are consistent with the  $\chi$ EFT computations of PNM (see Fig. 1) which were used to tune the CDFs in Ref. [24]. The difference in the conclusions arises from the fact that our collection includes EoS with small values of the slope of symmetry energy, e.g.,  $(Q_{\text{sat}}, L_{\text{sym}}) \approx (-600, 30)$  MeV, which are still consistent with the  $\chi$ EFT band. This is in contrast, the collection of Ref. [24] which is limited to larger values of  $L_{\text{sym}} \approx 40$  MeV. Anticipating the discussion in the next section, we point out here that if the  $\Delta$ -resonance threshold is low enough, their nucleation relieves further the tension between the observations and CDF-based models.

### 3.2. CSs with heavy baryons

Next, we consider models which allow for the nucleation of heavy baryons in dense matter. The hyperonic EoS models that support massive two-solar mass CSs require the nucleonic sector to be a priori stiff, which results in a large radius of a canonical-mass star  $R_{1.4} \gtrsim 13$  km [36, 37, 60–64]. Only during recent years, hyperon- $\Delta$  admixed CDF-based models were developed which were compatible with the nuclear data, radius measurements of CSs, and the tidal deformability inferred from the analysis of the GW170817 event [31, 47, 65–67]. The appearance of  $\Delta$ -resonances, in parallel with hyperons, does not affect the maximum mass of a static CS, but reduces the radius of the star by tens of percent, depending on the value of  $\Delta$ -potential in nuclear matter  $U_{\Delta}$ . Therefore, it is convenient for further discussion to denote underlying EoS model by the potential of  $\Delta$ 's, whereby the parameters specifying the nucleonic and hyperonic sectors are fixed.

In Fig. 3 we present the  $M$ - $R$  relations for purely nucleonic, hyperonic, and hyperon- $\Delta$  admixed stellar matter for several parameter values, along with current astrophysical observational constraints. In panel (a) the EoS models are constructed from nucleonic model with  $Q_{\text{sat}} = 600$  MeV, SU(6) symmetric parameterization for the hyperonic sector which results in a maximum mass  $M_{\text{max}} \approx 2.0 M_{\odot}$ , and a SU(3) symmetric parameterization which yields  $M_{\text{max}} \approx 2.3 M_{\odot}$ . To assess the range of variations in the sequences arising from the uncertainties in  $\Delta$  potential  $U_{\Delta}$  and the value of  $L_{\text{sym}}$  in nucleonic sector which are crucial for the radius of the star, we consider for each model  $U_{\Delta}/U_N = 1, 4/3$ , and  $5/3$  for  $L_{\text{sym}} = 30, 60$  MeV. In panel (b) we present results for alternative EoS models which are constructed from nucleonic model has  $Q_{\text{sat}} = -200$  MeV in combination with a SU(3) symmetric model for the hyperonic sector, which gives  $M_{\text{max}} \approx 2.0 M_{\odot}$ .

In Fig. 3 (a), we show the results for the nucleonic model with  $(Q_{\text{sat}}, L_{\text{sym}}) = (600, 30)$  MeV which are marginally compatible with the CCO in HESS J1731-347 constraint at 95.4% CI limit. Allowing for hyperons and  $\Delta$ -resonances and varying the value of  $U_{\Delta}$  we observe the reduction of the stellar radius with increasing value of  $U_{\Delta}$ . The  $M$ - $R$  track in this case could lie within the 68.3% CI ellipse. For a (isovector) stiffer nucleonic EoS model with  $(Q_{\text{sat}}, L_{\text{sym}}) = (600, 60)$  MeV which produces  $M$ - $R$  tracks outside the HESS J1731-347 region, the onset of hyperons and resonances leads to  $M$ - $R$  tracks that are within 95.4% CI region if a sufficiently attractive  $\Delta$  potential is chosen, e.g.,  $U_{\Delta}/U_N = 5/3$ . In Fig. 3 (b), for EoS models that are constructed from a (isoscalar) softer nucleonic model with  $Q_{\text{sat}} = -200$  MeV, the allowed range for  $L_{\text{sym}}$  is enlarged from  $L_{\text{sym}} \lesssim 40$  MeV in purely nucleonic models to  $L_{\text{sym}} \lesssim 80$  MeV in heavy baryons admixed models. We thus conclude that the tight constraint on the value of  $L_{\text{sym}}$  set by requirement of their compatibility with HESS J1731-347, is relaxed by about 30–40 MeV if nucleation of heavy baryons in dense matter is allowed. Even though such models help to reconcile the realistic values of  $L_{\text{sym}}$  with low-mass putative observations, it should



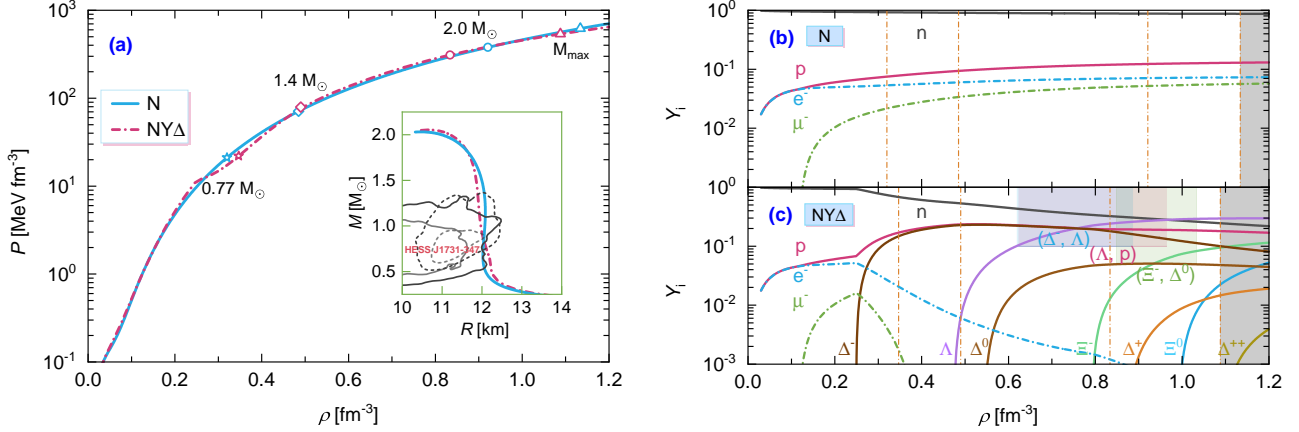


Figure 4: EoS and the corresponding particle fraction for nucleonic and hyperon- $\Delta$  admixed models that support a  $0.77 M_{\odot}$  CS with radius  $\sim 12.0$  km and a maximum mass of  $\sim 2.0 M_{\odot}$ . The nucleonic EoS corresponds to the pair  $(Q_{\text{sat}}, L_{\text{sym}}) = (-600, 40)$  MeV, while the hyperon- $\Delta$  admixed EoS is constructed from the nucleonic model with  $(Q_{\text{sat}}, L_{\text{sym}}) = (-200, 40)$  MeV, combined with a SU(3) symmetric parametrization of the hyperonic sector and  $U_{\Delta}/U_N = 5/3$  value of  $\Delta$  potential. In the left panel the positions of the respective  $0.77, 1.4, 2.0 M_{\odot}$  CSs and the maximum-mass configurations are marked by different symbols, while in the right panel, the corresponding central densities are indicated by thick vertical lines. In the right panel the gray shaded area shows the densities beyond the maximum-mass configurations. For hyperon- $\Delta$  admixed EoS model the regions of density where direct Urca processes are allowed are indicated by shadings with different colors.

be noted that if HESS J1731-347 is a baryonic star it contains likely only non-strange particles, due to its low mass. Indeed, as shown in Fig. 3, the onset of hyperons occurs in stars with larger mass with  $M \gtrsim 1.2 M_{\odot}$ .

### 3.3. Composition of the CCO in HESS J1731-347

Fig. 4 shows the EoS and composition for nucleonic and heavy baryon admixed models that support a  $0.77 M_{\odot}$  CS with radius  $\sim 12.0$  km and a maximum mass  $\sim 2.0 M_{\odot}$ . The nucleonic EoS has  $(Q_{\text{sat}}, L_{\text{sym}}) = (-600, 40)$  MeV; while the  $\Delta$ -admixed hyperonic EoS model has  $(Q_{\text{sat}}, L_{\text{sym}}) = (-200, 40)$  MeV, a SU(3) symmetric parameterization in the hyperonic sector and  $U_{\Delta}/U_N = 4/3$ . These two EoS models yield similar  $M$ - $R$  relations which are shown in the inset of Fig. 4(a), and the deviation in radius for a fixed mass is found less than 3%. For star with a mass  $\sim 0.77 M_{\odot}$ , the inner core density is about  $2\rho_{\text{sat}}$ , around where significant difference in particle composition is observed. Thus, the knowledge of the mass and radius alone does not allow one to distinguish the internal composition of CSs. In fact, even under the restrictive assumption of purely nucleonic stars, current empirical knowledge allows for multiple solutions for the composition of  $\beta$ -equilibrium matter, i.e., the composition of CSs cannot be determined unequivocally [68].

However, as well known, the particle content of dense matter is an important factor in the cooling of CSs due to new channels of neutrino emissions in the presence of heavy baryons. Because of same values of  $L_{\text{sym}}$  the nucleonic and heavy baryon admixed models lead to a similar composition at low density  $\rho \lesssim 0.25 \text{ fm}^{-3}$  in Figs. 4(b) and (c). We note that the requirement of a small radius of CCO in HESS J1731-347, and equivalently a low value of coefficient  $L_{\text{sym}}$  preclude the onset of the direct Urca process in such models. In contrast, in the  $\Delta$ -admixed hyperonic matter a trace fraction of hyperons and  $\Delta$ 's will open up a host of direct Urca processes involving these particles. According to Fig. 4(c) the  $\Delta$ -admixed hyperonic EoS allows the direct Urca processes in a large region of the density,

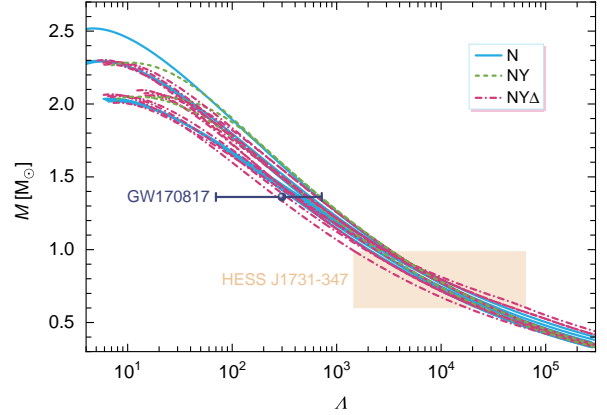


Figure 5: Mass-tidal deformability relation for various EoS models and matter compositions. The results are derived from a collection of our models that satisfy all relevant astrophysical constraints at 95.4% CI. These include nucleonic (N), hyperonic (NY), and hyperon- $\Delta$  admixed (NY $\Delta$ ) one. The constraint for a  $1.36 M_{\odot}$  star deduced from the analysis of GW170817 [9, 10] is shown for comparison. The mass range for a star with  $M = 0.77^{+0.20}_{-0.17} M_{\odot}$  corresponding to the inference for CCO in HESS J1731-347 [23] is indicated by shading.

$0.62$ - $1.03 \text{ fm}^{-3}$ , specifically  $\Delta^- \rightarrow \Lambda + e^- + \bar{\nu}_e$ ,  $\Lambda \rightarrow p + e^- + \bar{\nu}_e$ , and  $\Xi^- \rightarrow \Delta^0 + e^- + \bar{\nu}_e$ , are allowed and their thresholds are indicated in Fig. 4(c) as well. The onset of hyperons then will affect the cooling behaviour of stars more massive than HESS J1731-347, see Ref. [31] and references therein.

### 3.4. Tidal deformability and $I$ -Love- $Q$ relations

The gross quantities of a CS such as the mass, radius, deformability, moment of inertia, quadrupole moment, etc., sensitively depend on the microscopic EoS. In Fig. 5 we show the mass vs dimensionless tidal deformability relations for our models that satisfy all relevant astrophysical constraints at the 95.4% CI. All these models satisfy the constraint placed for a  $1.36 M_{\odot}$  star from the analysis of the GW170817 event. The ranges for the estimated mass  $M = 0.77^{+0.20}_{-0.17} M_{\odot}$  of CCO in

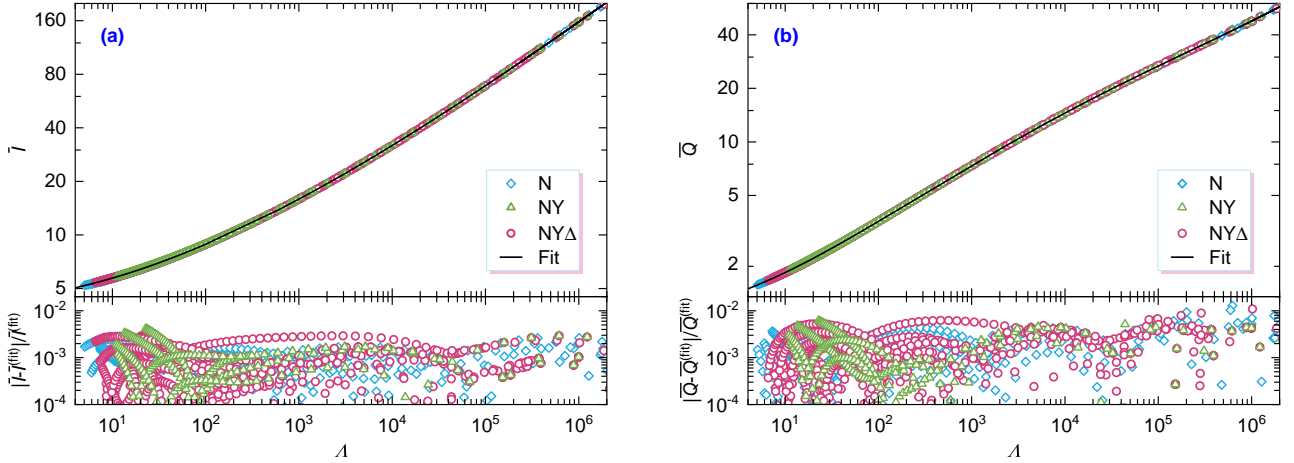


Figure 6: The  $I$ -Love and  $Q$ -Love relations for nonrotating CSs. The top panels show universal relations for various EoS models and matter compositions, together with fitting curves; bottom panels show fractional errors between the fitting curves and numerical results. The results are derived from a collection of valid models that satisfy all relevant astrophysical constraints at the 95.4% CI for the cases of nucleonic ( $N$ ), hyperonic ( $NY$ ), and hyperon- $\Delta$  admixed ( $NY\Delta$ ) compositions.

Table 1: The coefficients of the fit formulas of the  $I$ -Love- $Q$  relations.

	$\bar{I}$ - $\Lambda$	$\bar{Q}$ - $\Lambda$	$\bar{I}$ - $\bar{Q}$
$a_0$	$1.48978 \times 10^0$	$1.84748 \times 10^{-1}$	$1.28033 \times 10^0$
$a_1$	$6.45216 \times 10^{-2}$	$1.01466 \times 10^{-1}$	$8.81910 \times 10^{-1}$
$a_2$	$2.12766 \times 10^{-2}$	$4.48923 \times 10^{-2}$	$-2.92930 \times 10^{-1}$
$a_3$	$-5.95664 \times 10^{-4}$	$-3.87686 \times 10^{-3}$	$1.42509 \times 10^{-1}$
$a_4$	$5.15851 \times 10^{-6}$	$1.07983 \times 10^{-4}$	$-1.56774 \times 10^{-2}$

HESS J1731-347 are indicated as well. Since the low-mass stars have very large tidal deformability  $\Lambda$ , spanning the range from  $10^3$  to  $10^5$ , it is clear that they could be good targets for GW observatories if involved in a merger process.

Various approximately universal relations connecting different CS properties have been established and intensively studied in recent years. Of particular interest is the  $I$ -Love- $Q$  relations that first discovered in Ref. [69] which connect the dimensionless moment of inertia  $\bar{I}$ , tidal deformability  $\Lambda$ , and the spin-induced quadrupole moment  $\bar{Q}$  of neutron stars in slow rotation approximation. These relations can be numerically described with a polynomial [69, 70]:

$$\ln y = a_0 + a_1 \ln x + a_2 (\ln x)^2 + a_3 (\ln x)^3 + a_4 (\ln x)^4, \quad (7)$$

where pairs  $(x, y)$  represent  $(\Lambda, \bar{I})$ ,  $(\Lambda, \bar{Q})$  and  $(\bar{Q}, \bar{I})$ . These relations are commonly studied for stars with mass  $M \gtrsim 1.0 M_\odot$  [70].

Here we briefly investigate whether these relations hold for stars with heavy baryons, in particular, the hyperon- $\Delta$  admixed CSs, especially in the low-mass region extending down to about  $0.2 M_\odot$ . Our results for  $I$ -Love and  $Q$ -Love relations, derived from a collection of our models that satisfy all relevant astrophysical constraints at the 95.4% CI, are shown in Fig. 6, together with the fits according to Eq. (7), where the bottom panels present the fractional differences between the data and the fits. It is seen in Fig. 6 that the absolute fractional differences are  $\lesssim 1\%$  for all two relations. Clearly, the universality holds for the third pair  $\bar{I}$ - $\bar{Q}$  as well. The best-fit coefficients with Eq. (7)

for the three relations are summarized in Table 1, which are consistent with those found in Ref. [70]. Thus, our results extend the previously reported universal  $I$ -Love- $Q$  relations for CSs into the low-mass domain.

#### 4. Summary

In this work, we have studied the problem of the nature of the CCO in HESS J1731-347 by using a CDF approach for dense matter with and without heavy baryons in high-density regions. While some authors suggested the “strange star” scenario for this object [25, 26], here we explore a “less strange” alternative. The density functional we used was parameterized and varied via two parameters - the skewness coefficient  $Q_{\text{sat}}$  of symmetric nuclear matter and the slope coefficient  $L_{\text{sym}}$  of the symmetry energy. The hyperon potentials were tuned to the most plausible potentials extracted from hypernuclear data. The  $\Delta$ -potential was taken to be in the range  $1 \leq U_\Delta/U_N \leq 5/3$ , — a reasonable range consistent with the current data.

We found that purely nucleonic models for the EoS can accommodate the estimate for mass and radius of the CCO in HESS J1731-347, but only if the slope of symmetry energy coefficient  $L_{\text{sym}}$  is fairly small, i.e.,  $L_{\text{sym}} \lesssim 60$  MeV for models with  $Q_{\text{sat}} \sim -600$  MeV, and  $L_{\text{sym}} \lesssim 30$  MeV for models with  $Q_{\text{sat}} \sim 600$  MeV. These low values for  $L_{\text{sym}}$  are compatible with the analysis of the PREX-II and CREX experiments of neutron skins, dipole polarizabilities, as well as recent  $\chi$ EFT computations. Allowing for hyperon and  $\Delta$ -resonance populations in dense matter, our EoS models allow a broader range of values of  $L_{\text{sym}}$ . We note that these models do allow for maximum masses in the range  $2.0 M_\odot \lesssim M_{\text{max}} \lesssim 2.3 M_\odot$ .

Another important point of our analysis is that our EoS models with or without heavy baryons which predict very similar  $M$ - $R$  relations have different compositions with different sets of neutrino emission processes and, therefore, cooling behavior. The core matter of nucleonic CS does not allow for the direct Urca process, as the low values of coefficient  $L_{\text{sym}}$  used in our

models result in a low proton fraction. Note that the DDME2 parametrization, i.e., without variations of the  $L_{\text{sym}}$  parameter does not allow direct Urca as well. In the case of the  $\Delta$ -admixed hyperonic matter, direct Urca processes involving  $\Delta$ 's and hyperons are allowed for a large region of the density relevant for high mass CSs. Finally, we showed that the presence of heavy baryons in CSs does not alter the universalities of the  $I$ -Love- $Q$  relations for static configurations. We further extended this relation to the low-mass domain not been studied previously, but which is relevant for the CCO in HESS J1731-347. These relations were found accurate up to 1% for mass range from  $0.2$ - $2.5 M_{\odot}$ .

## Acknowledgements

J. L. acknowledges the support of the NNSF of China (No. 12105232), the Fundamental Research Funds for the Central Universities (No. SWU-020021), and by the Venture & Innovation Support Program for Chongqing Overseas Returnees (No. CX2021007). A. S. is supported by the Deutsche Forschungsgemeinschaft Grant No. SE 1836/5-2 and the Polish NCN Grant No. 2020/37/B/ST9/01937 at Wrocław University.

## References

- [1] H. T. Cromartie, E. Fonseca, S. M. Ransom, et al., Relativistic Shapiro delay measurements of an extremely massive millisecond pulsar, *Nat. Astron.* 4 (2020) 72–76. [arXiv:1904.06759](#), [doi:10.1038/s41550-019-0880-2](#).
- [2] E. Fonseca, H. T. Cromartie, T. T. Pennucci, et al., Refined Mass and Geometric Measurements of the High-mass PSR J0740+6620, *Astrophys. J. Lett.* 915 (2021) L12. [arXiv:2104.00880](#), [doi:10.3847/2041-8213/ac03b8](#).
- [3] R. W. Romani, D. Kandel, A. V. Filippenko, T. G. Brink, W. Zheng, PSR J0952–0607: The Fastest and Heaviest Known Galactic Neutron Star, *Astrophys. J. Lett.* 934 (2022) L18. [arXiv:2207.05124](#), [doi:10.3847/2041-8213/ac8007](#).
- [4] T. E. Riley, A. L. Watts, S. Bogdanov, et al., A *NICER* View of PSR J0030+0451: Millisecond Pulsar Parameter Estimation, *Astrophys. J. Lett.* 887 (2019) L21. [arXiv:1912.05702](#), [doi:10.3847/2041-8213/ab481c](#).
- [5] M. C. Miller, F. K. Lamb, A. J. Dittmann, et al., PSR J0030+0451 Mass and Radius from *NICER* Data and Implications for the Properties of Neutron Star Matter, *Astrophys. J. Lett.* 887 (2019) L24. [arXiv:1912.05705](#), [doi:10.3847/2041-8213/ab50c5](#).
- [6] T. E. Riley, A. L. Watts, P. S. Ray, et al., A *NICER* View of the Massive Pulsar PSR J0740+6620 Informed by Radio Timing and XMM-Newton Spectroscopy, *Astrophys. J. Lett.* 918 (2021) L27. [arXiv:2105.06980](#), [doi:10.3847/2041-8213/ac0a81](#).
- [7] M. C. Miller, F. K. Lamb, A. J. Dittmann, et al., The Radius of PSR J0740+6620 from *NICER* and XMM-Newton Data, *Astrophys. J. Lett.* 918 (2021) L28. [arXiv:2105.06979](#), [doi:10.3847/2041-8213/ac089b](#).
- [8] B. P. Abbott, R. Abbott, T. D. Abbott, et al., GW170817: Observation of Gravitational Waves from a Binary Neutron Star Inspiral, *Phys. Rev. Lett.* 119 (2017) 161101. [arXiv:1710.05832](#), [doi:10.1103/PhysRevLett.119.161101](#).
- [9] B. P. Abbott, R. Abbott, T. D. Abbot, et al., GW170817: Measurements of neutron star radii and equation of state, *Phys. Rev. Lett.* 121 (2018) 161101. [arXiv:1805.11581](#), [doi:10.1103/PhysRevLett.121.161101](#).
- [10] B. P. Abbott, R. Abbott, T. D. Abbot, et al., Properties of the binary neutron star merger GW170817, *Phys. Rev. X* 9 (2019) 011001. [arXiv:1805.11579](#), [doi:10.1103/PhysRevX.9.011001](#).
- [11] S. De, D. Finstad, J. M. Lattimer, et al., Tidal Deformabilities and Radii of Neutron Stars from the Observation of GW170817, *Phys. Rev. Lett.* 121 (2018) 091102. [arXiv:1804.08583](#), [doi:10.1103/PhysRevLett.121.091102](#).
- [12] M. W. Coughlin, T. Dietrich, Z. Doctor, et al., Constraints on the neutron star equation of state from AT2017gfo using radiative transfer simulations, *Mon. Not. R. Astron. Soc.* 480 (2018) 3871–3878. [arXiv:1805.09371](#), [doi:10.1093/mnras/sty2174](#).
- [13] K. Kiuchi, K. Kyutoku, M. Shibata, K. Taniguchi, Revisiting the lower bound on tidal deformability derived by AT 2017gfo, *Astrophys. J. Lett.* 876 (2019) L31. [arXiv:1903.01466](#), [doi:10.3847/2041-8213/ab1e45](#).
- [14] M. Soares-Santos, D. E. Holz, J. Annis, et al., The Electromagnetic Counterpart of the Binary Neutron Star Merger LIGO/Virgo GW170817. I. Discovery of the Optical Counterpart Using the Dark Energy Camera, *Astrophys. J. Lett.* 848 (2017) L16. [arXiv:1710.05459](#), [doi:10.3847/2041-8213/aa9059](#).
- [15] V. A. Villar, J. Guillochon, E. Berger, et al., The Combined Ultraviolet, Optical, and Near-Infrared Light Curves of the Kilonova Associated with the Binary Neutron Star Merger GW170817: Unified Data Set, Analytic Models, and Physical Implications, *Astrophys. J. Lett.* 851 (2017) L21. [arXiv:1710.11576](#), [doi:10.3847/2041-8213/aa9c84](#).
- [16] M. Shibata, S. Fujibayashi, K. Hotokezaka, et al., Modeling GW170817 based on numerical relativity and its implications, *Phys. Rev. D* 96 (2017) 123012. [arXiv:1710.07579](#), [doi:10.1103/PhysRevD.96.123012](#).
- [17] B. Margalit, B. D. Metzger, Constraining the Maximum Mass of Neutron Stars From Multi-Messenger Observations of GW170817, *Astrophys. J. Lett.* 850 (2017) L19. [arXiv:1710.05938](#), [doi:10.3847/2041-8213/aa991c](#).
- [18] M. Ruiz, S. L. Shapiro, A. Tsokaros, GW170817, General Relativistic Magnetohydrodynamic Simulations, and the Neutron Star Maximum Mass, *Phys. Rev. D* 97 (2018) 021501. [arXiv:1711.00473](#), [doi:10.1103/PhysRevD.97.021501](#).
- [19] L. Rezzolla, E. R. Most, L. R. Weih, Using gravitational-wave observations and quasi-universal relations to constrain the maximum mass of neutron stars, *Astrophys. J. Lett.* 852 (2018) L25. [arXiv:1711.00314](#), [doi:10.3847/2041-8213/aaa401](#).
- [20] M. Shibata, E. Zhou, K. Kiuchi, S. Fujibayashi, Constraint on the maximum mass of neutron stars using GW170817 event, *Phys. Rev. D* 100 (2019) 023015. [arXiv:1905.03656](#), [doi:10.1103/PhysRevD.100.023015](#).
- [21] S. Khadkikar, A. R. Raduta, M. Oertel, A. Sedrakian, Maximum mass of compact stars from gravitational wave events with finite-temperature equations of state, *Phys. Rev. C* 103 (2021) 055811. [arXiv:2102.00988](#), [doi:10.1103/PhysRevC.103.055811](#).
- [22] P. S. Shternin, D. D. Ofengeim, W. C. G. Ho, et al., Model-independent constraints on superfluidity from the cooling neutron star in Cassiopeia A, *Mon. Not. R. Astron. Soc.* 506 (2021) 709–726. [arXiv:2106.05692](#), [doi:10.1093/mnras/stab1695](#).
- [23] V. Doroshenko, V. Suleimanov, G. Pühlhofer, A. Santangelo, A strangely light neutron star within a supernova remnant, *Nat. Astron.* 6 (2022) 1444–1451. [doi:10.1038/s41550-022-01800-1](#).
- [24] L. Brodie, A. Haber, Nuclear and Hybrid Equations of State in Light of the Low-Mass Compact Star in HESS J1731-347, *arXiv e-prints* (2023) [arXiv:2302.02989](#)[arXiv:2302.02989](#), [doi:10.48550/arXiv.2302.02989](#).
- [25] F. Di Clemente, A. Drago, G. Pagliara, Is the compact object associated with HESS J1731-347 a strange quark star?, *arXiv e-prints* (2022) [arXiv:2211.07485](#)[arXiv:2211.07485](#), [doi:10.48550/arXiv.2211.07485](#).
- [26] J. E. Horvath, L. S. Rocha, L. M. de Sá, et al., A light strange star in the remnant HESS J1731–347: Minimal consistency checks, *Astron. Astrophys.* 672 (2023) L11. [arXiv:2303.10264](#), [doi:10.1051/0004-6361/202345885](#).
- [27] Y. Suwa, T. Yoshida, M. Shibata, H. Umeda, K. Takahashi, On the minimum mass of neutron stars, *Mon. Not. R. Astron. Soc.* 481 (2018) 3305–3312. [arXiv:1808.02328](#), [doi:10.1093/mnras/sty2460](#).
- [28] J. G. Martinez, K. Stovall, P. C. C. Freire, et al., Pulsar J0453+1559: A Double Neutron Star System with a Large Mass Asymmetry, *Astrophys. J.* 812 (2015) 143. [arXiv:1509.08805](#), [doi:10.1088/0004-637X/812/2/143](#).



- [29] F. Özel, P. Freire, Masses, Radii, and the Equation of State of Neutron Stars, *Ann. Rev. Astron. Astrophys.* 54 (2016) 401–440. [arXiv:1603.02698](#), [doi:10.1146/annurev-astro-081915-023322](#).
- [30] M. Oertel, M. Hempel, T. Klähn, S. Typel, Equations of state for supernovae and compact stars, *Rev. Mod. Phys.* 89 (1) (2017) 015007. [arXiv:1610.03361](#), [doi:10.1103/RevModPhys.89.015007](#).
- [31] A. Sedrakian, J. J. Li, F. Weber, Heavy baryons in compact stars, *Prog. Part. Nucl. Phys.* 131 (2023) 104041. [arXiv:2212.01086](#), [doi:10.1016/j.pnpnp.2023.104041](#).
- [32] G. A. Lalazissis, T. Nikšić, D. Vretenar, P. Ring, New relativistic mean-field interaction with density-dependent meson-nucleon couplings, *Phys. Rev. C* 71 (2005) 024312. [doi:10.1103/PhysRevC.71.024312](#).
- [33] V. Pascalutsa, M. Vanderhaeghen, S. N. Yang, Electromagnetic excitation of the Delta(1232)-resonance, *Phys. Rep.* 437 (2007) 125–232. [arXiv:hep-ph/0609004](#), [doi:10.1016/j.physrep.2006.09.006](#).
- [34] B. D. Serot, J. D. Walecka, Recent progress in quantum hadrodynamics, *Int. J. Mod. Phys. E* 6 (1997) 515–631. [arXiv:nucl-th/9701058](#), [doi:10.1142/S0218301397000299](#).
- [35] J. Schaffner, C. B. Dover, A. Gal, et al., Multiply strange nuclear systems, *Ann. Phys.* 235 (1994) 35–76. [doi:10.1006/aphy.1994.1090](#).
- [36] M. Oertel, C. Providência, F. Gulminelli, A. R. Raduta, Hyperons in neutron star matter within relativistic mean-field models, *J. Phys. G* 42 (2015) 075202. [arXiv:1412.4545](#), [doi:10.1088/0954-3889/42/7/075202](#).
- [37] J. J. Li, W. H. Long, A. Sedrakian, Hypernuclear stars from relativistic Hartree-Fock density functional theory, *Eur. Phys. J. A* 54 (2018) 133. [arXiv:1801.07084](#), [doi:10.1140/epja/i2018-12566-6](#).
- [38] J. Margueron, R. Hoffmann Casali, F. Gulminelli, Equation of state for dense nucleonic matter from metamodelling. II. Predictions for neutron star properties, *Phys. Rev. C* 97 (2018) 025806. [arXiv:1708.06895](#), [doi:10.1103/PhysRevC.97.025806](#).
- [39] J. J. Li, A. Sedrakian, Constraining compact star properties with nuclear saturation parameters, *Phys. Rev. C* 100 (2019) 015809. [arXiv:1903.06057](#), [doi:10.1103/PhysRevC.100.015809](#).
- [40] A. Feliciello, T. Nagae, Experimental review of hypernuclear physics: recent achievements and future perspectives, *Rep. Prog. Phys.* 78 (2015) 096301. [doi:10.1088/0034-4885/78/9/096301](#).
- [41] A. Gal, E. V. Hungerford, D. J. Millener, Strangeness in nuclear physics, *Rev. Mod. Phys.* 88 (2016) 035004. [arXiv:1605.00557](#), [doi:10.1103/RevModPhys.88.035004](#).
- [42] J. K. Ahn, H. Akikawa, S. Aoki, et al., Double- $\Lambda$  hypernuclei observed in a hybrid emulsion experiment, *Phys. Rev. C* 88 (2013) 014003. [doi:10.1103/PhysRevC.88.014003](#).
- [43] A. Drago, A. Lavagno, G. Pagliara, D. Pigato, Early appearance of  $\Delta$  isobars in neutron stars, *Phys. Rev. C* 90 (2014) 065809. [arXiv:1407.2843](#), [doi:10.1103/PhysRevC.90.065809](#).
- [44] A. R. Raduta,  $\Delta$ -admixed neutron stars: Spinodal instabilities and dUrca processes, *Phys. Lett. B* 814 (2021) 136070. [arXiv:2101.03718](#), [doi:10.1016/j.physletb.2021.136070](#).
- [45] G. Baym, C. Pethick, P. Sutherland, The ground state of matter at high densities: equation of state and stellar models, *Astrophys. J.* 170 (1971) 299.
- [46] G. Baym, H. A. Bethe, C. J. Pethick, Neutron star matter, *Nucl. Phys. A* 175 (1971) 225–271.
- [47] J. J. Li, A. Sedrakian, Implications from GW170817 for  $\Delta$ -isobar Admixed Hypernuclear Compact Stars, *Astrophys. J. Lett.* 874 (2019) L22. [arXiv:1904.02006](#), [doi:10.3847/2041-8213/ab1090](#).
- [48] S. Huth, C. Wellenhofer, A. Schwenk, New equations of state constrained by nuclear physics, observations, and QCD calculations of high-density nuclear matter, *Phys. Rev. C* 103 (2021) 025803. [arXiv:2009.08885](#), [doi:10.1103/PhysRevC.103.025803](#).
- [49] N.-B. Zhang, B.-A. Li, J. Xu, Combined Constraints on the Equation of State of Dense Neutron-rich Matter from Terrestrial Nuclear Experiments and Observations of Neutron Stars, *Astrophys. J.* 859 (2018) 90. [arXiv:1801.06855](#), [doi:10.3847/1538-4357/aac027](#).
- [50] R. Abbott, T. D. Abbott, S. Abraham, et al., GW190814: Gravitational Waves from the Coalescence of a 23 Solar Mass Black Hole with a 2.6 Solar Mass Compact Object, *Astrophys. J. Lett.* 896 (2020) L44. [arXiv:2006.12611](#), [doi:10.3847/2041-8213/ab960f](#).
- [51] F. J. Fattoyev, C. J. Horowitz, J. Piekarewicz, B. Reed, GW190814: Impact of a 2.6 solar mass neutron star on the nucleonic equations of state, *Phys. Rev. C* 102 (2020) 065805. [arXiv:2007.03799](#), [doi:10.1103/PhysRevC.102.065805](#).
- [52] A. Sedrakian, F. Weber, J. J. Li, Confronting GW190814 with hyperonization in dense matter and hypernuclear compact stars, *Phys. Rev. D* 102 (2020) 041301. [arXiv:2007.09683](#), [doi:10.1103/PhysRevD.102.041301](#).
- [53] J. J. Li, A. Sedrakian, F. Weber, Rapidly rotating  $\Delta$ -resonance-admixed hypernuclear compact stars, *Phys. Lett. B* 810 (2020) 135812. [arXiv:2010.02901](#), [doi:10.1016/j.physletb.2020.135812](#).
- [54] D. Adhikari, H. Albatineh, D. Androic, et al., Accurate determination of the neutron skin thickness of  $^{208}\text{Pb}$  through parity-violation in electron scattering, *Phys. Rev. Lett.* 126 (2021) 172502. [arXiv:2102.10767](#), [doi:10.1103/PhysRevLett.126.172502](#).
- [55] B. T. Reed, F. J. Fattoyev, C. J. Horowitz, J. Piekarewicz, Implications of PREX-2 on the equation of state of neutron-rich matter, *Phys. Rev. Lett.* 126 (2021) 172503. [arXiv:2101.03193](#), [doi:10.1103/PhysRevLett.126.172503](#).
- [56] P.-G. Reinhard, X. Roca-Maza, W. Nazarewicz, Information Content of the Parity-Violating Asymmetry in  $^{208}\text{Pb}$ , *Phys. Rev. Lett.* 127 (2021) 232501. [arXiv:2105.15050](#), [doi:10.1103/PhysRevLett.127.232501](#).
- [57] D. Adhikari, H. Albatineh, D. Androic, et al., Precision Determination of the Neutral Weak Form Factor of  $^{48}\text{Ca}$ , *Phys. Rev. Lett.* 129 (2022) 042501. [arXiv:2205.11593](#), [doi:10.1103/PhysRevLett.129.042501](#).
- [58] P.-G. Reinhard, X. Roca-Maza, W. Nazarewicz, Combined Theoretical Analysis of the Parity-Violating Asymmetry for  $^{48}\text{Ca}$  and  $^{208}\text{Pb}$ , *Phys. Rev. Lett.* 129 (2022) 232501. [arXiv:2206.03134](#), [doi:10.1103/PhysRevLett.129.232501](#).
- [59] C. Drischler, R. J. Furnstahl, J. A. Melendez, D. R. Phillips, How Well Do We Know the Neutron-Matter Equation of State at the Densities Inside Neutron Stars? A Bayesian Approach with Correlated Uncertainties, *Phys. Rev. Lett.* 125 (2020) 202702. [arXiv:2004.07232](#), [doi:10.1103/PhysRevLett.125.202702](#).
- [60] S. Weissenborn, D. Chatterjee, J. Schaffner-Bielich, Hyperons and massive neutron stars: the role of hyperon potentials, *Nucl. Phys. A* 881 (2012) 62–77. [arXiv:1111.6049](#), [doi:10.1016/j.nuclphysa.2012.02.012](#).
- [61] S. Weissenborn, D. Chatterjee, J. Schaffner-Bielich, Hyperons and massive neutron stars: vector repulsion and SU(3) symmetry, *Phys. Rev. C* 85 (2012) 065802. [arXiv:1112.0234](#), [doi:10.1103/PhysRevC.85.065802](#).
- [62] G. Colucci, A. Sedrakian, Equation of state of hypernuclear matter: impact of hyperon–scalar-meson couplings, *Phys. Rev. C* 87 (2013) 055806. [arXiv:1302.6925](#), [doi:10.1103/PhysRevC.87.055806](#).
- [63] L. Tolos, M. Centelles, A. Ramos, Equation of State for Nucleonic and Hyperonic Neutron Stars with Mass and Radius Constraints, *Astrophys. J.* 834 (2017) 3. [arXiv:1610.00919](#), [doi:10.3847/1538-4357/834/1/3](#).
- [64] M. Fortin, S. S. Avancini, C. Providência, I. Vidaña, Hypernuclei and massive neutron stars, *Phys. Rev. C* 95 (2017) 065803. [arXiv:1701.06373](#), [doi:10.1103/PhysRevC.95.065803](#).
- [65] J. J. Li, A. Sedrakian, F. Weber, Competition between delta isobars and hyperons and properties of compact stars, *Phys. Lett. B* 783 (2018) 234–240. [arXiv:1803.03661](#), [doi:10.1016/j.physletb.2018.06.051](#).
- [66] P. Ribes, A. Ramos, L. Tolos, C. Gonzalez-Boquera, M. Centelles, Interplay between  $\Delta$  Particles and Hyperons in Neutron Stars, *Astrophys. J.* 883 (2019) 168. [doi:10.3847/1538-4357/ab3a93](#).
- [67] J. J. Li, A. Sedrakian, M. Alford, Relativistic hybrid stars with sequential first-order phase transitions and heavy-baryon envelopes, *Phys. Rev. D* 101 (2020) 063022. [arXiv:1911.00276](#), [doi:10.1103/PhysRevD.101.063022](#).
- [68] C. Mondal, F. Gulminelli, Can we decipher the composition of the core of a neutron star?, *Phys. Rev. D* 105 (2022) 083016. [arXiv:2111.04520](#), [doi:10.1103/PhysRevD.105.083016](#).
- [69] K. Yagi, N. Yunes, I-Love-Q: Unexpected Universal Relations for Neutron Stars and Quark Stars, *Science* 341 (2013) 365–368. [arXiv:1302.4499](#), [doi:10.1126/science.1236462](#).
- [70] K. Yagi, N. Yunes, Approximate Universal Relations for Neutron Stars and Quark Stars, *Phys. Rep.* 681 (2017) 1–72. [arXiv:1608.02582](#), [doi:10.1016/j.physrep.2017.03.002](#).